Estratto da:

OPERA IPOGEA

Journal of Speleology in Artificial Cavities

1-2 / 2023

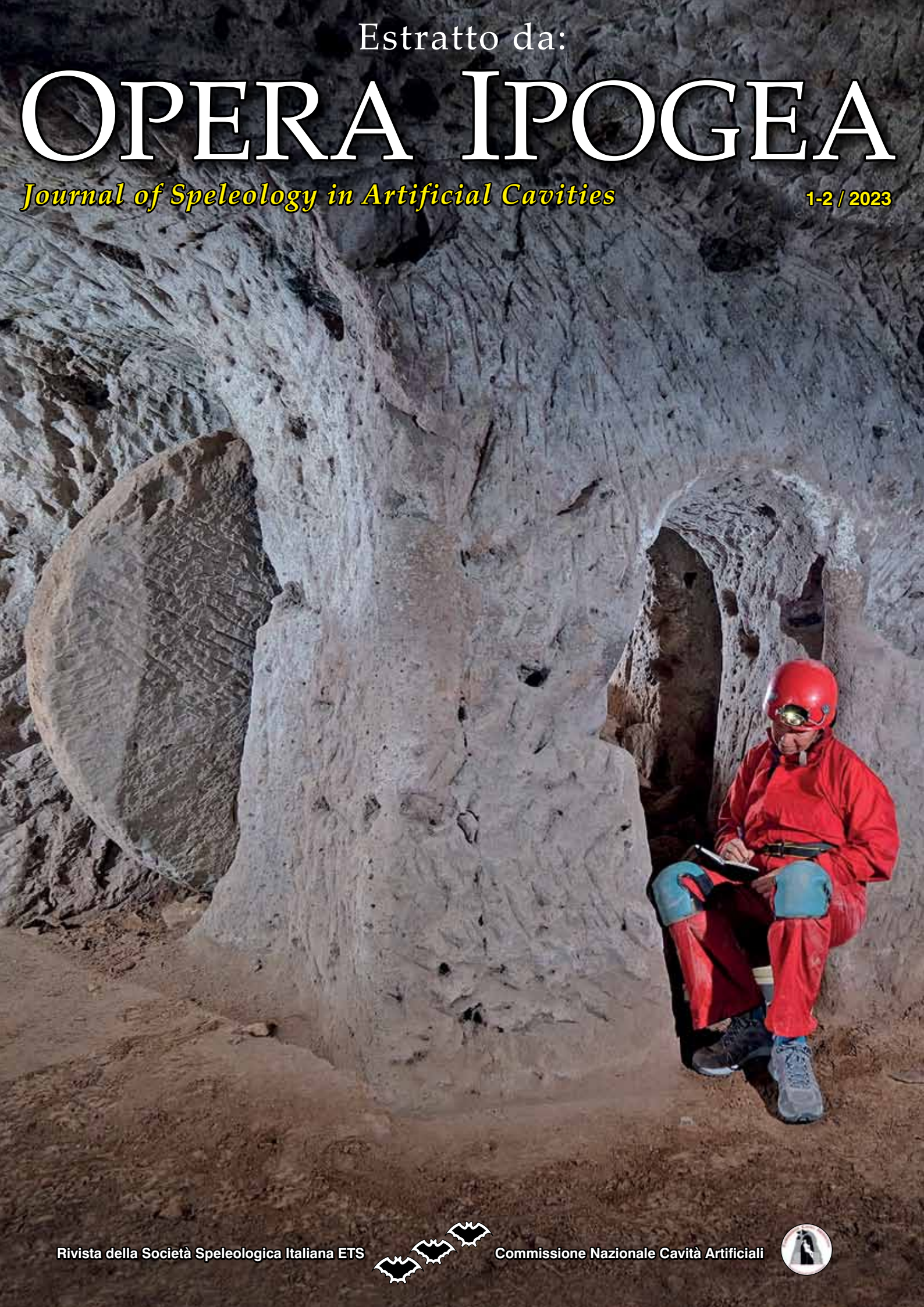

Rivista della Società Speleologica Italiana ETS

Commissione Nazionale Cavità Artificiali

Indice

Indice

Indice

Segnalibri

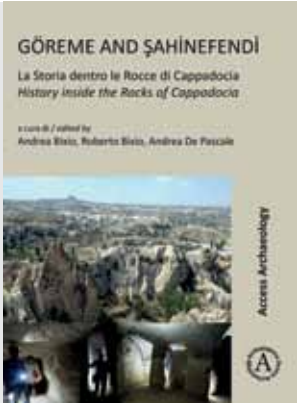

OPERA IPOGEA

Journal of Speleology in Artificial Cavities

Memorie della Commissione Nazionale Cavità Artificiali

Autorizzazione del Tribunale di Bologna n. 7702 dell'11 ottobre 2006

Rivista Semestrale della Società Speleologica Italiana ETS

ISSN 1970-9692 / DOI https://doi.org/10.57588/SSIOI1/2/2023

www.operaipogea.it operaipogea

Rivista dell'Area 10 "Scienze dell'antichità, filologico-letterarie e storico-artistiche"
classificata dell'Agenzia Nazionale di Valutazione del Sistema Universitario e della Ricerca (ANVUR)
quale rivista scientifica rilevante ai fini dell'Abilitazione Scientifica Nazionale (ASN)

Redazione
c/o Studio Saj / Corso Magenta 29/2, 16125 Genova - Italia

Composizione e impaginazione
Luca Paternoster, Stefano Saj

Anno XXV / Numero 1-2 / 2023

Foto di copertina
Rifugio sotterraneo presso il villaggio rupestre di Dimitre (Kayseri, Turchia) (foto R. Straub)

Foto quarta di copertina
Grande ambiente scavato nella falesia del villaggio rupestre
di Dimitre (Kayseri, Turchia) (foto A. E. Keskin)

Acquisti e abbonamenti dal numero 1/2024
https://www.lerma.it/catalogo/rivista/239

Per acquisto numeri 1999-2023 (salvo disponibilità)
biblioteca@socissi.it - contabilita@socissi.it

Tipografia
Conigraf Srl - Viserba (RN)

Comparative analysis of different techniques for the topographic survey of artificial galleries: the case study of the INGV Messina headquarter geophysical tunnel (Sicily, Italy)

Analisi comparativa di differenti tecniche di rilievo topografico di gallerie artificiali: il caso di studio del tunnel geofisico della sede INGV di Messina

Paolo Madonia[1], Marianna Cangemi[2], Marcello D'Agostino[2], Gaetano Giudice[3], Danilo Messina[3,4]

Abstract

Here we present the comparative analysis of different techniques based on: 1) a composite system integrating laser range meter, laser level and electronic compass implemented on smartphones; 2) the Disto X system; 3) the Lidar on board of iPhones; 4) the laser scanner BLK 360 G1. We tested these methods in the INGV Messina (Italy) headquarter geophysical tunnel. Thanks to the very shallow depth of the tunnel, it was possible locating with a differential GNSS receiver the starting and final points of the hypogeum, using these as control points for calibrating the different surveys. The comparison among the different survey methods suggests that methods based on magnetic angle measurements could be affected by significant errors, due to the presence of metallic materials in the built environment, and that the Lidar implemented in iPhones does not give accurate quantitative results, if not adequately corrected with more performing methods, like Terrestrial Laser Scanners.

Keywords: GNSS, iPhone, Laser level, Laser range meter, Lidar.

Riassunto

Nel presente lavoro vengono presentati i risultati di un'analisi comparata di quattro diversi metodi di rilievo di cavità sotterranee: 1) un sistema topografico composito, risultante dall'integrazione di un distanziometro laser, una livella laser e la bussola elettronica integrata su smartphone; 2) il Disto X; 3) il sistema Lidar integrato negli iPhone Pro; 4) il laser scanner terrestre BLk 360 G1. L'area test selezionata è stata una galleria artificiale destinata ad ospitare strumentazione geofisica, ubicata all'interno della sede di Messina dell'Istituto Nazionale di Geofisica e Vulcanologia. La peculiarità di questa galleria è la sua ubicazione sub-superficiale, con una camera terminale la cui volta a cupola emerge dalla superficie del suolo, della quale è stato possibile ubicare con precisione, tramite GNSS differenziale, la culminazione. Questa è stata poi proiettata sul pavimento della galleria sotterranea, utilizzando un filo a piombo, materializzando un caposaldo su cui appoggiare un rilievo ipogeo, effettuato con un livello ottico, ed utilizzato come riferimento per verificare la precisione delle restituzioni dei dati acquisiti con le 4 metodologie sotto test.
Dal punto di vista planimetrico, il confronto tra i quattro rilievi ha evidenziato come quelli basati su misure angolari tramite bussola elettronica, ossia il topografico composito ed il Disto X, presentassero errori significativi dovuti alle interferenze tra i materiali metallici presenti all'interno della struttura in cemento armato della galleria. Ne consegue che, in caso di rilievi di ipogei artificiali che si sviluppano all'interno di rocce contenenti minerali magnetici o paramagnetici, ovvero in ambienti

[1] Istituto Nazionale di Geofisica e Vulcanologia, Sezione di Catania – OE, OBS & Earth Lab, Via Portera 10, 90015 Cefalù (Italy)
[2] Istituto Nazionale di Geofisica e Vulcanologia, Sezione di Catania – OE, Sede di Messina, Viale Regina Margherita 18, 98121 Messina (Italy)
[3] Istituto Nazionale di Geofisica e Vulcanologia, Sezione di Catania – OE, Piazza Roma 2, 95125 Catania (Italy)
[4] Università di Palermo, Dipartimento di Scienze della Terra e del Mare, Via Archirafi 22, 90123 Palermo (Italy)
Corresponding author: Paolo Madonia - paolo.madonia@ingv.it

urbanizzati con presenza di strutture in cemento armato o condotte metalliche, sia più opportuno effettuare rilievi tramite strumentazione ottica (come ad esempio i livelli da cantiere).
Il rilievo effettuato con il Lidar implementato all'interno dell'iPhone ha mostrato errori pari al 2,6% delle lunghezze battute, che li rendono inidonei a posizionamenti su cartografie in scala maggiore di 1:5000, dovuti sia alla qualità, commerciale e non professionale, del sensore, sia alla generazione di sdoppiamenti delle nuvole di punti, che ne causano una traslazione progressiva. I dati generati dal laser scanner terrestre (TLS), ossia il BLK, mostrano invece una perfetta rispondenza con il rilievo da livello ottico, evidenziando come tali sistemi siano estremamente affidabili per generare modelli 3D di ambienti ipogei. Va evidenziato che i 4 rilievi sottoposti a test non sono stati georeferenziati utilizzando come punto di controllo la proiezione del punto relativo alla volta della camera terminale, ma esclusivamente altri punti di controllo posti all'imbocco della galleria, sempre ubicati tramite GNSS: questo per non falsare i risultati del test, destinato a fornire informazioni utili per il rilievo di gallerie ipogee che, dopo l'ingresso, non abbiano altri punti certi localizzabili in superficie.

Parole chiave: Distanziometro laser, GNSS, iPhone, Lidar, Livella laser.

Introduction

The advent of Global Navigation Satellite Systems (GNSS) and Terrestrial Laser Scanners (TLS) opened a new era in the topographic survey of natural and artificial caves, giving an unprecedented opportunity of acquiring huge georeferenced point clouds in short times. Between the years 1998 and 2000 two important milestones were reached in the development of these applications. In 1998 the first TLS effectively usable for underground surveys came to the market, although first experimental applications dated 1988 (Oludare Idrees and Pradhan, 2016). In May 2000 former USA President Bill Clinton decided to eliminate the Selective Availability distortion from GPS signals, allowing non-military users to use stand-alone GPS receivers for locating points with errors of few meters <https://gisgeography.com/selective-availability-gps/, last accessed 02.11.2023>.
Since then, the progressive cost reduction of this instrumentation boosted their use in the survey of caves: among many others, see the papers from Cosso et al. (2014), Giordan et al. (2021) or Pukanská et al. (2020). Anyway, the real turning point in the widespread diffusion of TLS was the implementation of sensors in consumer-grade devices: in 2020 Apple™ integrated a native LIDAR sensor in the iPhone 12 Pro smartphone series (and also on iPad Pro). The availability of a low cost, ruggedized and light commercial device, integrating a GNSS module, an inertial platform and a Lidar sensor, has opened new frontiers in indoor environment modelling in general, and topographic survey of underground, often hostile, environments in particular (Tavani et al., 2022; Teo and Yang, 2023).
Examples on the use of iPhone Lidar for the 3D reconstruction of artificial caves can be found in the work of Rutkowski et al. (2023), who used this device for modelling a mine shaft in Poland, or in Ferrari (2023), who modelled the Flavian amphitheatre cisterns at Pozzuoli (Italy), and in Zago et al. (2023), who retrieved the digital model of an old aqueduct in Asolo (Italy).
Two orders of problems arise while using this technology in the survey of underground, GNSS signals denied, spaces: the accuracy of absolute global, and relative local, positioning of point clouds.
Really, the former is a false problem, because the customer-grade GNSS boards, equipping smartphones, are able to give positions with errors of few meters (if good satellite configurations are present), namely with an accuracy compatible with the typical tolerances of regional technical maps, acquired at the nominal scale of 1:5,000 or 1:10,000. Problems could be encountered for restitutions at more detailed scales, like 1:2,000 or higher: in this case, the use of more precise differential GNSS receivers is required, for correctly locating the external Ground Control Points (GCP) adopted for georeferencing the point clouds from Lidar.
On the contrary, the crucial question is the evaluation of the error affecting the reciprocal distances of the points of the Lidar clouds in the 3D space, particularly critical for objects with a longitudinal dimension markedly predominant with respect to the others, like galleries. If intermediate GCPs cannot be determined, positioning error propagation can lead to significant distortions of the reconstructed objects.
With the aim of comparing different methodologies, characterized by very different costs and expected precisions, we carried out a multiple survey in a shallow artificial tunnel, about 40 m long, located in the premises of the INGV headquarter of Messina (Italy), and built for hosting geophysical instrumentation in its terminal chamber. The cup-shaped vault of the chamber emerges from the ground, giving the opportunity of precisely locating it and using its centre as a GCP for evaluating the overall error of the surveys.

Site description

The test site for the comparison of the different survey techniques was an artificial tunnel, about 40 m long and made of reinforced concrete, built at few tents of cm under the ground, inside an embankment in the premises of the INGV headquarter of Messina (Italy) (fig. 1a, b). The tunnel, about 2.4 m wide and 3 m high, has a barrel vault and it is thermically isolated by two thin internal masonry walls, presently partially collapsed, leaving a 20 cm gap between them and the main concrete walls (fig. 1c). The tunnel leads to an internal circular chamber (fig. 1e), with a diameter of

Fig.. 1 – From the top to the bottom, and from left to right: a location of the gallery and its planimetry (background image from Google Earth); b entrance of the gallery; c internal view of the gallery during topographic survey operations; d particular of the topographic survey system; e the final circular room, aimed to host geophysical instrumentation; f the cupule of the final room outcropping from the ground (*draft by M. Cangemi)*.

Fig. 1 – Dall'alto verso il basso, e da sinistra verso destra: a ubicazione della galleria e sua planimetria (l'immagine di sfondo da Google Earth); b entrata della galleria; c vista interna della galleria durante le operazioni di rilievo topografico; d particolare del Sistema di rilevamento topografico; e la stanza terminale circolare, destinata ad ospitare strumentazione geofisica; f la cupola della stanza finale che emerge dalla superficie topografica (disegno di M. Cangemi).

5 m. It is thermically decoupled from the main concrete structure by an internal thin wall, creating a 0.5 m gap, which exchange air with the exterior through 8 vertical pipes (10 cm diameter), whose exits are disposed all around the cup-shaped vault of the chamber, emerging from the ground (fig. 1f). Two different structures, aimed to host geophysical sensors, were created inside the chamber: a plinth and a marble work bench (fig. 1a), both physically decoupled from the chamber floor for not transmitting vibrations to the sensors.

Survey methods and related data processing

We executed 4 different surveys, based on: i) A consumer-grade topographic system composed of a range meter Bosch Zamo, a laser level Stanley® Cubix™, the electronic compass utility implemented in the iPhone XR, a Bosch level staff and a 5 m metric tape; ii) The Disto X 4 system; iii) The Lidar implemented in the iPhone 15 Pro; iv) The BLK 360 G1 system. The first two are systems made for acquiring polar coordinates (distance and azimuthal and zenithal angles), while the other two are TLS with a different grade of performance.

The migration from relative local to absolute geographic coordinates, namely the georeferencing process, was based on 4 GCPs (fig. 1a) whose positions were determined by a Trimble R6 L1L2 differential GNSS, connected to the Trimble Italia permanent GNSS network, operating in RTK mode with horizontal and vertical precisions better than 2 and 3 cm, respectively. The vertical projection of GCP4 on the underground circular chamber floor (fig.1a,e) was determined by a plumb line introduced from a hole in the outcropping cupule (fig.1f). We adopted the global coordinate system WGS84 UTM zone 33N, EPSG Code 32633.

For assembling the topographic system, we mounted on a topographic tripod the laser level, blocking over this the iPhone used for azimuthal angle determination. Aluminium and plastic are the dominant materials used for the laser level case, the tripod and the blocking system, but we preliminary checked, targeting a fixed point with the level switched on, that this assemblage did not produce any angular deviation in the iPhone compass measurements.

The main advantage of this method, which materializes a horizontal reference line collimated on the staff level, kept vertical thanks to a spherical level mounted on it (fig. 1c, d), is that only azimuthal angular measurements are needed. As well known, the main source of errors in cave surveys is the measurement of angles by handled compasses and clinometers. With our system, elevation variations are given by metric measures, subtracting the height of the laser trace, read on the staff level, from the height of the laser emitter. Moreover, the azimuthal angle is read on a compass fixed on a tripod and perfectly collimated on a target, avoiding errors introduced by its free-handling. The assembled system on operation is illustrated in fig. 1d. It is important to remind that azimuthal angles read on the electronic compass must be corrected for the local magnetic declination at the time of the survey, prior to report the data on a base map.

Disto X is a well-known system used for the topographic survey of caves, based on a laser range meter Leica Disto A3, modified inserting a compass and clinometric electronic board. The device is equipped with a Bluetooth connection system, for transferring to PDAs or smartphones all the acquired measures (Heeb, 2008).

Lidar sensors were introduced in the "Pro" versions of Apple iPhones since 2020. These sensors operate in the near infrared (NIR) spectrum and emit a laser from a VCSEL (Vertical Cavity Surface Emitting Laser) in a 2D array. VCSELs are suitable for mobile devices because they have small size and low power consumption relative to the power output (Khaldi et al., 2020). The direct time of flight (dTOF) of the pulses emitted by the VCSEL is measured with a Single Photon Avalanche Photodiode (SPAD) (Niclass et al., 2020; Bruschini et al., 2019).

The VECSEL has a maximum range of 5 m and emits an array containing 8x8 points that is diffracted into a 3x3 grid, generating a total of 576 points.

We used an iPhone 15 Pro to perform the survey. The device, released in September 2023, has a weight of 187 g, a 6.1" screen, a A17 Pro chip (3 nm dimension) with 6-core CPU with 2 performance cores and 4 efficiency cores, 6-core GPU, 16-core Neural Engine, 8 GB RAM, 128 GB memory and IOS 17.1 software version <https://www.apple.com/iphone-15-pro/specs/, last accessed 10.11.2023>. The device has 3 RGB cameras: a 48MP main camera, a 12MP Ultra-Wide camera, a 12MP 3x Telephoto camera, and a Lidar sensor. The software used for point cloud acquisition was the 3D Scanner App, version 2.0.17 by Laan Labs <https://3dscannerapp.com, last accessed 11.11.2023>. We used the "Point Cloud" scanning mode, and the scanning was conducted by walking inside the tunnel with the iPhone in hand by rotating it in circular motions so as to capture the entire surroundings. The Lidar sensor and cameras were facing the entire time toward the bottom of the tunnel, where the survey began, and continued backward to the exit. The acquisition that lasted about 5 minutes, resulted in a point cloud that we exported in the .E57 format.

The exported data were processed with the open-source software CloudCompare, version 2.12.4 <http://www.cloudcompare.org, last accessed 10.11.2023>. CloudCompare is a free software (GNU License) for Windows, IOS and Linux platforms, which processes point clouds and triangular meshes. It originated to compare point clouds from laser scanner surveys, and was later implemented into point cloud processing software with some rather advanced algorithms. GCPs were imported in CloudCompare, and the Align tool was used for georeferencing the point cloud in the global coordinate system.

TLS, on the other hand, allow the surface of an ele-

ment to be reconstructed in 3-D using the emission of a laser beam from a static point, and the detection of the latter reflected on the target to calculate the distance between the object and the sensor (Pfiefer and Briese, 2007; Petrie and Toth, 2008; Heritage and Large, 2009).

TLS typically use an infrared wavelength laser beam that can be emitted continuously (phase-shift method), or as a pulse (time-of-flight or pulse-based method, Petrie and Toth, 2008; Deems et al., 2013). Each reflection of the laser beam creates a 3-D point in the space around the scanner, producing a point cloud representing the surface of the scanned object. The density and spacing of the points theoretically depend on the resolution of the scan, with the optimal resolution representing a trade-off between the largest number of points, required for the purpose of the project, and the duration of the scan. Resolution is an instrument parameter that affects scan times: higher resolutions require longer scan times.

We chose to use the Leica TLS BLK 360 G1 to capture reference data. This system, working with the time-of-flight (TOF) technology, can capture 360,000 points per second, using a laser beam in the near-infrared wavelength (830 nm), with an accuracy of 7 mm at a distance of 20 m, and an acquisition range of 0.6 m to 60 m. The device has a height of 0.165 m, a diameter of 0.1 m and weighs 1 kg. The scanner rotates along its vertical axis, capturing data at 360° horizontally and 300° vertically; this does not allow individual scans to capture information in the nadir direction <https://shop.leica-geosystems.com/it/it-IT/leica-blk/blk360/blk360-g1-overview, last accessed 11.11.2023>

Nine scanning stations were carried out by placing the instrument close to the targets so that the location of the targets within the point cloud was detectable.

We used the Leica Cyclon Field 360 software to set the scanning parameters, start the scans, and perform preliminary scans registration in the field. For all scans, we set *HDR* and the *"High density"* scan mode, which takes 6' 40 s to acquire data for each scan.

The entire acquisition of all nine scans, including data transfer and alignment of the scans on the software, took about 3 hours.

After data acquisition, the primary processing was performed almost fully automatically with Cyclone Register 360 software (BLK Edition), where the alignment between scans was done through a fully automated process based on the automatic "cloud-to-cloud" approach. The point cloud was registered in the global coordinate system using the coordinates of the three GCPs located outside (GCP1, GCP2, GCP3) and was exported in .E57 format.

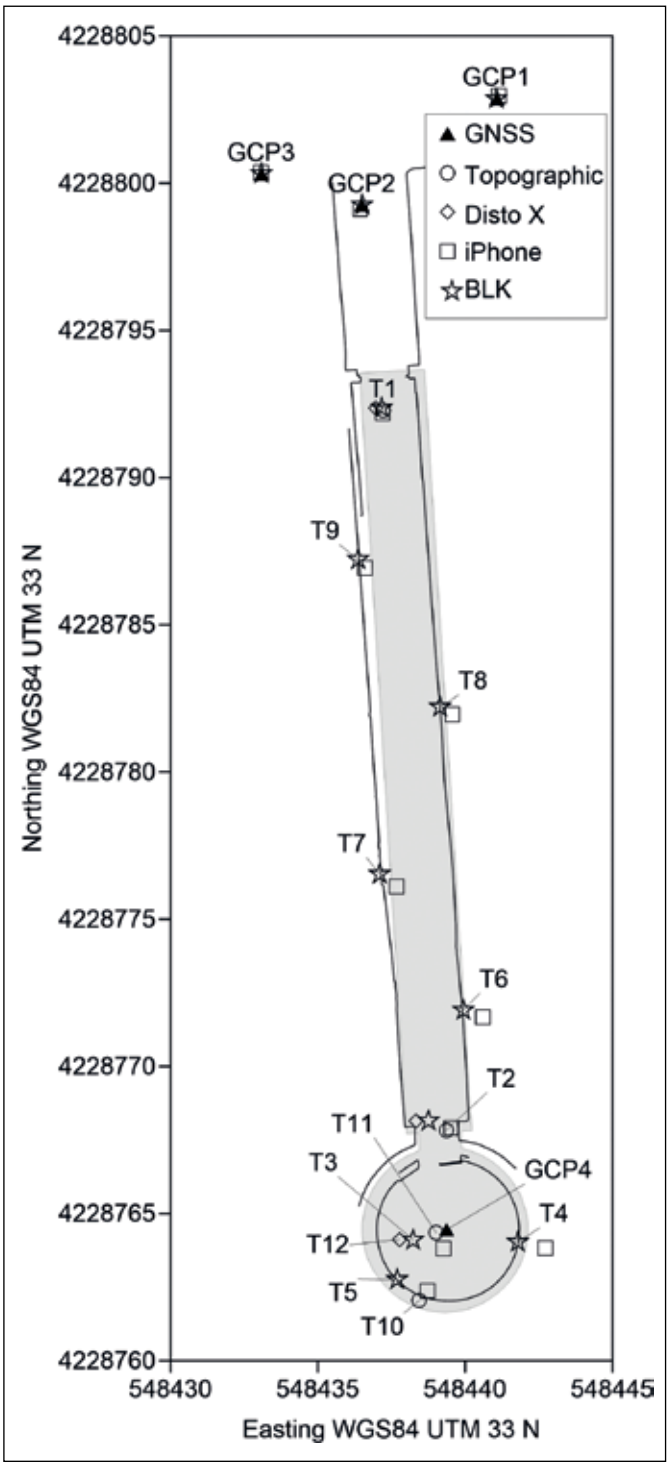

Fig. 2 – Positions of GCPs and targets acquired with the different methods. Boundaries of the galleries as from BLK survey (thick black line) and the previous topographical survey (grey filled polygon) are also represented (*draft by P. Madonia)*.

Fig. 2 – Posizione dei GCP e dei bersagli acquisiti con i diversi metodi. Sono inoltre rappresentati i limiti della galleria derivanti dal rilievo BLK (linea nera spessa) e dal precedente rilievo topografico (poligono grigio) (disegno di P. Madonia).

Comparative analysis of results

Positions of GCPs and targets, acquired with the different methodologies, are reported in table 1 and fig. 2, which also shows the internal walls of the gallery, as from the BLK survey (black tick line), and the overall planimetric projection of the gallery, as from a previous survey based on GNSS and optical levelling and ranging, integrated with metric tape measurements (light grey area). It is worth of note that, while the BLK image of the gallery was georeferenced using GCPs 1–3, that from the previous survey also

included GCP4, for constraining the position of the final part of the gallery.
A good superimposition of the gallery boundaries from BLK and the first topographical survey is highlighted by the map reported in fig. 2, with few tens of centimetres separating the two planimetries at the farer end of the final circular room (about 1% of the total flight distance from T1 to the end of the gallery).
Positions of targets from the topographical and Disto X surveys are more scattered, with differences up to several tents of centimetres. This scattering can be attributed to the disturbances induced by the metallic rebar of the reinforced concrete, used for building the gallery, which causes a diversion of the azimuthal angle measured by electronic compasses from the true magnetic north direction. The previous survey (grey filled polygon in fig. 2) was not affected by this error because based on relative angles, measured by an optical level, with respect to an initial alignment (two GCPs located by GNSS).

Id	Easting	Northing	Elevation (m)	Survey	E error	N error (m)	H error (m)
GCP1	548441.07	4228802.87	99.30	G,I,B	0.05	0.05	0.01
GCP2	548436.49	4228799.26	99.20	G,I,B	0.04	0.08	0.02
GCP3	548433.08	4228800.31	100.55	G,I,B	0.01	0.02	0.01
GCP4	548439.36	4228764.45	103.70	G,T	0.34	0.10	0.23
T1	548437.17	4228792.36	99.28	B,T,D,I,	0.12	0.08	0.09
T2	548438.75	4228768.15	99.59	B,T,D,I,	0.55	0.17	0.36
T3	548438.24	4228764.10	99.58	B,I	1.02	0.29	0.64
T4	548441.79	4228764.03	101.39	B,I	0.92	0.21	0.71
T5	548437.70	4228762.75	101.27	B,I	1.02	0.37	0.72
T6	548439.94	4228771.91	101.24	B,I	0.67	0.24	0.52
T7	548437.10	4228776.53	101.19	B,I	0.57	0.42	0.43
T8	548439.15	4228782.20	101.16	B,I	0.42	0.25	0.34
T9	548436.37	4228787.22	101.28	B,I	0.24	0.29	0.23
T10	548438.44	4228762.04	98.99	T	n.d.	n.d.	n.d.
T11	548439.02	4228764.34	98.91	T	n.d.	n.d.	n.d.
T12	548437.77	4228764.12	99.59	D	n.d.	n.d.	n.d.

Table 1 – Id, projected coordinates (UTM WGS84 33 N Zone), elevation (ellipsoidal) of GCPs and targets determined with different surveys: GNSS, Topographic, Disto X, iPhone, BLK; in case of multiple determinations the reported values are from the more precise method, indicated as the first of the list in the survey column. Errors are expressed as standard deviation for almost three different measures, as absolute differences if only two measures are available.

Tabella 1 – Identificativo, coordinate proiettate (UTM WGS84 Zona 33 N), quota (ellissoidica) dei GCP e dei bersagli, determinate con i differenti metodi: GNSS, Topografico, Disto X, iPhone, BLK. In caso di misure multiple il valore riportato è relativo al metodo più preciso, indicato come primo della lista nella colonna dei rilievi. Gli errori sono espressi in termini di deviazione standard, nel caso si abbiano almeno tre misure disponibili, come differenza assoluta tra le misure, se queste sono due.

Target positions retrieved by the iPhone were those affected by the highest errors, with divergences from the positions from BLK that exceeded 1 m (targets 3 and 5, table 1). If these errors are plotted versus the progressive flight distances from the first one (T1), as illustrated in Fig.3, a strong (r = 0.98) linear relationship is evidenced: divergence increases as the 2.6% of the distance. A similar relationship is also found for elevation errors (2.1% of the distance).
This is also caused, in addition to the lower accuracy of the iPhone Lidar compared to the BLK, by the creation of multiple surfaces in the point cloud by the iPhone. The iPhone survey, in fact, has a duplication of geometries at the tunnel entrance, which results in the elongation, and subsequent translation, of the point cloud along the longitudinal direction of the tunnel, which causes a larger error in the position of the targets (fig. 4).
We tried to align the point cloud generated by the iPhone with the point cloud generated by the BLK through a cloud-to-cloud approach. This prevented the presence of the multiple surfaces generated at the entrance, shown in fig. 4, to negatively affect the position of the targets inside the tunnel. This also enables the optimal orientation of the 3D model generated by the iPhone.
In this way the error increases on the three GCPs, which are thus not used for georeferencing the point cloud, but the position error on the targets located inside the tunnel decreases significantly (tab. 2).

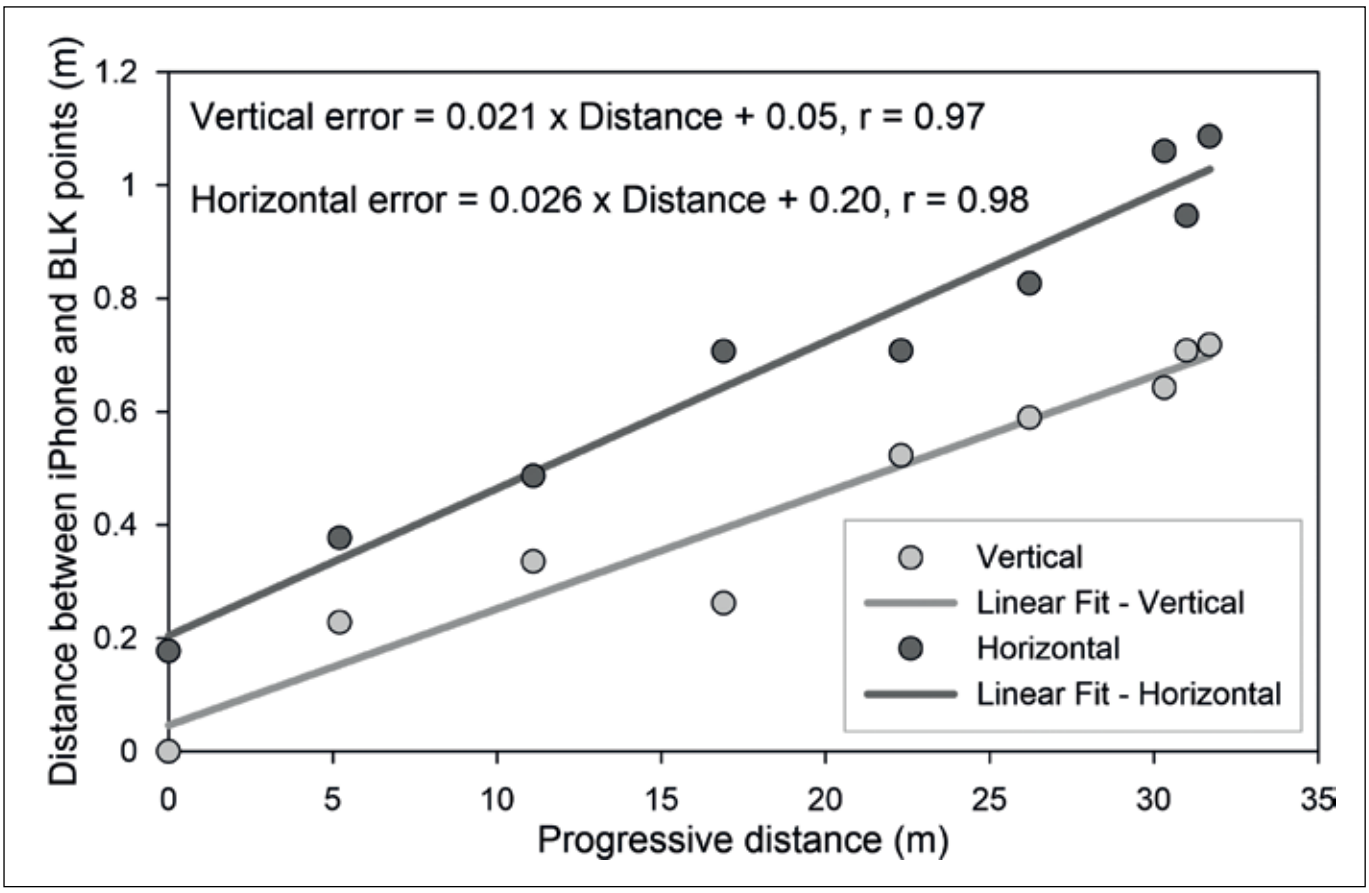

Fig. 3 – Horizontal and vertical divergences between target positions acquired by BLK and iPhone, plotted versus their progressive flight distances (*draft by P. Madonia)*.

Fig. 3 – Divergenze orizzontali e verticali tra le posizioni dei bersagli acquisite tramite BLK ed iPhone, riportate rispetto alle distanze progressive di rilievo (disegno di P. Madonia).

Id	Easting	Northing	Elevation	$E_{residual}$	$N_{residual}$	$Elevation_{residual}$
GCP1	548441,06	4228802,86	99,30	-0.33	-0.30	0.02
GCP2	548436,51	4228799,26	99,20	-0.06	-0.23	0.04
GCP3	548433,08	4228800,32	100,55	-0.13	-0.51	0.06
T1	548437,17	4228792,36	99,28	0.03	-0.17	0.00
T2	548438,75	4228768,15	99,59	-0.01	-0.04	0.00
T3	548438,24	4228764,10	99,58	-0.11	-0.02	-0.02
T4	548441,79	4228764,03	101,39	0.01	-0.01	0.01
T5	548437,70	4228762,75	101,27	-0.05	0.04	0.02
T6	548439,94	4228771,91	101,24	0.03	-0.05	-0.01
T7	548437,10	4228776,53	101,19	-0.01	0.04	0.01
T8	548439,15	4228782,20	101,16	-0.02	-0.06	0.01
T9	548436,37	4228787,22	101,28	0.01	-0.11	0.02

Table 2 – Results of the alignment of the iPhone survey on the BLK one: Id, projected coordinates, elevation (ellipsoidal) of GCPs and targets, determined with the BLK 360. Residuals are expressed as the absolute difference between measurements performed with the BLK and those performed with the iPhone, after the alignment. All values are in m.

Tabella 2 – Risultato dell'allineamento dei punti acquisiti con iPhone con quelli dal BLK: identificativo, coordinate proiettate, quota (ellissoidica) dei GCP e dei bersagli, determinate con il BLK. I residui sono espressi come differenza assoluta tra le misure effettuate con il BLK e quelle effettuate con l'iPhone, dopo l'allineamento. Tutti i valori sono in m.

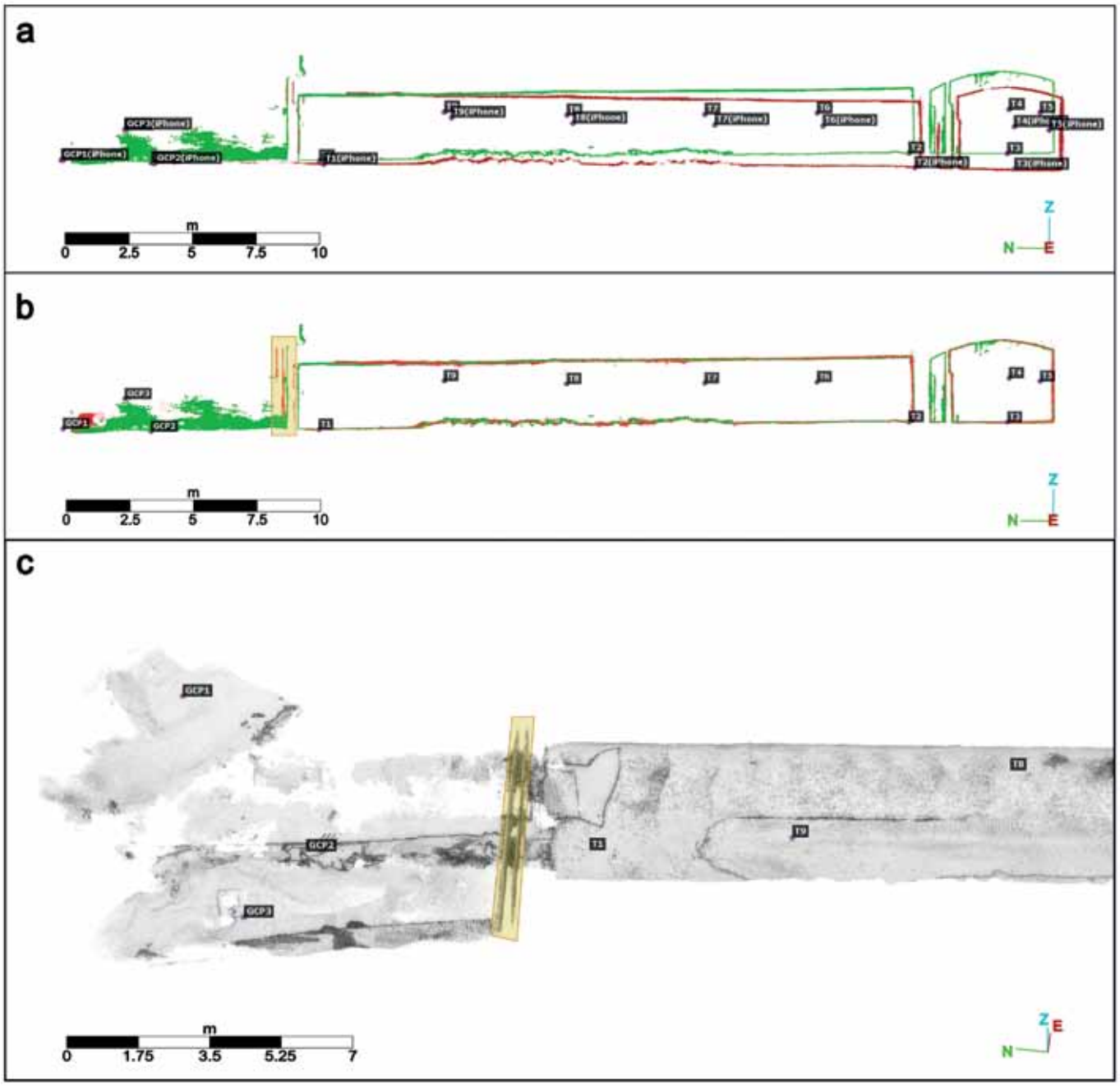

Fig. 4 – Point clouds generated by the BLK360 and the iPhone; a green cross section of the point cloud generated by the BLK360, in red cross section of the point cloud generated with the iPhone and georeferenced with the three external ground control points (GCP1, GCP2, GCP3); b green cross section of the point cloud generated by the BLK360, red cross section of the point cloud generated with the iPhone and aligned via the cloud to cloud approach to the BLK360 cloud, the yellow box indicates the area where some surfaces were duplicated by the iPhone; c shaded view of the iPhone point cloud, yellow duplicated surfaces (draft by D. Messina).

Fig. 4 – Nuvole di punti generate dal BLK360 e dall'iPhone; a in verde sezione trasversale della nuvola di punti generata dal BLK360, in rosso sezione trasversale della nuvola di punti generata con l'iPhone e georeferenziata con i tre ground control point esterni (GCP1, GCP2, GCP3); b in verde sezione trasversale della nuvola di punti generata dal BLK360, in rosso sezione trasversale della nuvola di punti generata con l'iPhone ed allineata tramite l'approccio cloud to cloud alla nuvola del BLK360, il riquadro giallo indica la zona dove sono state duplicate alcune superfici dall'iPhone; c vista ombreggiata della nuvola di punti dell'iPhone, in giallo le superfici duplicate (disegno di D. Messina).

It is worth of note that, while the cost of an iPhone equipped with a Lidar is cheaper than 1,500 €, that of the BLK is more than an order of magnitude greater, namely about 14,000 € for the hardware, plus about 1,500 €/year for a software licence: consequently, the use of a system that needs a much more expensive one for reaching acceptable precisions, seems nonsensical.

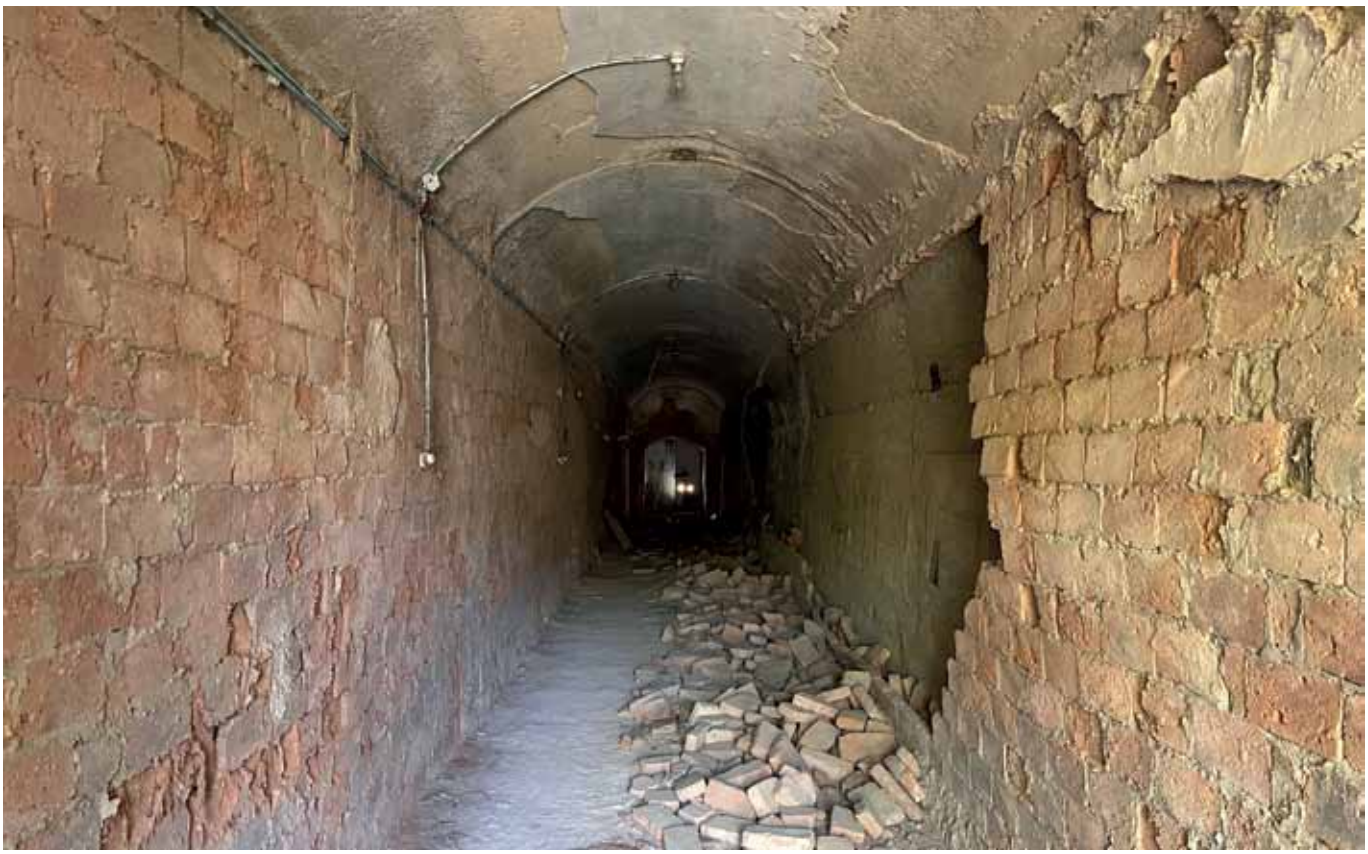

Fig. 5 – View of the tunnel from the entrance. In evidence, the masonry partition wall used for creating the air shaft, partially collapsed as shown in the right side of the photo (photo M. Cangemi).

Fig. 5 – Immagine del tunnel ripreso dall'ingresso. In evidenza, nella parte destra della foto, il tramezzo in mattoni utilizzato per creare l'intercapedine isolante, ed ora parzialmente crollato (foto M. Cangemi).

About elevation errors, while it was possible the evaluation of relative differences between BLK and iPhone, the only method for which it was possible estimating them with respect to GCPs is the topographic one, because GCP4 was projected on the gallery floor using a plumb line (see methods). As illustrated in tab. 1, the error was 0.23 m, less than 1% of the total flight distance among the targets.

Conclusions

Resuming the main findings arising from data discussion, the following evaluations can be proposed:
-Methods based on angular measurements by electronic compasses could be affected by significant errors if operations are carried out in modern built environments, characterized by the wide use of metallic paramagnetic materials. In this case, surveys should be carried out using optical systems measuring relative angles;
-The Lidar of iPhones or iPads suffer from some problems that cause multiple surfaces to be created. These could be used expeditiously to create semi-quantitative 3D models of underground voids such as tunnels, but it must be verified that multiple surfaces have not been generated within the model;
-Point clouds acquired along a gallery by high performance TLS, like the BLK, and georeferenced using only GCPs located at its entrance, give positions as precise as those obtained by topographic methods, confirming that TLS are very powerful instruments for creating 3D models of underground voids.

Acknowledgments

This study is a part of the activity of the Work Package 5 "NEMESIS" of the PNRR Project "MEET", coordinated by INGV. M. Cangemi and P. Madonia acquired and processed GNSS and topographic data, G. Giudice and D. Messina acquired and processed BLK, iPhone and Disto X data, M. D'Agostino supported field operations. Writing by P. Madonia and D. Messina. All authors contributed to the revision and final editing of the manuscript.

References

Bruschini C., Homulle H., Antolovic I. M., Burri S., Charbon E., 2019, *Single-photon avalanche diode imagers in biophotonics: review and outlook,* in Light: Science & Applications, 8(1), 87.

Cosso T., Ferrando I., Orlando A., 2014, *Surveying and mapping a cave using 3D laser scanner: the open challenge with free and open source software. The International Archives of the Photogrammetry*, in Remote Sensing and Spatial Information Sciences, Volume XL-5, ISPRS Technical Commission V Symposium, 23-25 June 2014, Riva del Garda, Italy, doi: 10.5194/isprsarchives-XL-5-181-2014.

Deems J. S., Painter T. H., Finnegan D. C., 2013, *Lidar measurement of snow depth: a review*, in Journal of Glaciology, 59(215), pp. 467-479.

Ferrari G., 2023, *The Pozzuoli (Naples, Italy) Flavian Amphitheatre cisterns: a basic experience in 3D modelling with LIDAR*, in Saj S., Galeazzi C., Betti M., Faccini F., Madonia P. (eds), proceedings of IV International Congress of Speleology in Artificial Cavities "Hypogea2023" (Genoa, Italy,29 September-1 October, 2023), Opera Ipogea, supplement to issue 1-2/2023, Società Speleologica Italiana ETS, Bologna, pp. 319-324.

Giordan D., Godone D., Baldo M., Piras M., Grasso N., Zerbetto R., 2021, *Survey Solutions for 3D Acquisition and Representation of Artificial and Natural Caves,* in Appl. Sci., 11, 6482. https://doi.org/10.3390/app11146482

Heeb B., 2008, *Paperless Caving – An Electronic Cave Surveying System*, in Proceedings of the IV European Speleological Congress, p. 130 – 133, France.

Heritage G., Large A., 2009, *Laser Scanning for the Environmental Sciences*. Wiley Blackwell, London, 288 pages. https://doi.org/10.1002/9781444311952

Khaldi A., Daniel E., Massin L., Kärnfelt C., Ferranti F., Lahuec C., ... & De Bougrenet de la Tocnaye J. L., 2020, A laser emitting contact lens for eye tracking. Scientific reports, 10(1), 14804.

Niclass C. L., Shpunt A., Agranov G. A., Waldon M. C., Rezk M. A., & Oggier T., 2020, *U.S. Patent No. 10,795,001*. Washington, DC: U.S. Patent and Trademark Office.

Oludare Idrees M., Pradhan B., 2016, *A decade of modern cave surveying with terrestrial laser scanning: A review of sensors, method and application development,* in International Journal of Speleology, 45 (1), pp. 71-88. Tampa, FL.

Petrie G., Toth C. K., 2018, *Introduction to laser ranging, profiling, and scanning*, in Topographic laser ranging and scanning, pp. 1-28, CRC Press.

Pfeifer N., Briese C., 2007, *Geometrical aspects of airborne laser scanning and terrestrial laser scanning. International Archives of Photogrammetry,* in Remote Sensing and Spatial Information Sciences, 36(3/W52), pp. 311-319.

Pukanská K., Bartoš K., Bella P., Gašinec J., Blistan P., Kovanic L., 2020, *Surveying and High-Resolution Topography of the Ochtiná Aragonite Cave Based on TLS and Digital Photogrammetry* in Appl. Sci., 10, 4633; doi: 10.3390/app10134633

Rutkowski W., Lipecki T, 2023, *Use of the iPhone 13 Pro LiDAR Scanner for Inspection and Measurement in the Mineshaft Sinking Process,* in Remote Sens., 15, 5089. https://doi.org/10.3390/rs15215089

Tavani S., Billi A., Corradetti A., Mercuri M., Bosman A., Cuffaro M., Seers T., Carminati E., 2022, *Smartphone assisted fieldwork: Towards the digital transition of geoscience fieldwork using LiDAR-equipped iPhones*, in Earth-Science Reviews, Volume 227, 103969, https://doi.org/10.1016/j.earscirev.2022.103969

Teo T. A., Yang C.-C., 2023, *Evaluating the accuracy and quality of an iPad Pro's built-in lidar for 3D indoor mapping*, in Developments in the Built Environment 14, 100169, https://doi.org/10.1016/j.dibe.2023.100169

Zago M., Davolio D, M., Pellegrini M., Sordi R., Sordi M., 2023. *The ancient aqueducts of Asolo (Italy): new investigations and acquisitions*, Saj S., Galeazzi C., Betti M., Faccini F., Madonia P. (eds), proceedings of IV International Congress of Speleology in Artificial Cavities "Hypogea2023" (Genoa, Italy,29 September-1 October, 2023), Opera Ipogea, supplement to issue 1-2/2023, Società Speleologica Italiana ETS, Bologna, pp. 99-106.